Earth Syst. Sci. Data, 17, 277–292, 2025
https://doi.org/10.5194/essd-17-277-2025


Open Access Earth System Science Data

# The high-resolution global shipping emission inventory by the Shipping Emission Inventory Model (SEIM)

**Wen Yi[1,★], Xiaotong Wang[2,★], Tingkun He[1], Huan Liu[1], Zhenyu Luo[1], Zhaofeng Lv[1], and Kebin He[1]**

[1]State Key Joint Laboratory of ESPC, School of Environment, Tsinghua University, Beijing 100084, China
[2]Key Laboratory of Beijing on Regional Air Pollution Control,
Beijing University of Technology, Beijing 100124, China
★These authors contributed equally to this work.

**Correspondence:** Huan Liu (liu_env@tsinghua.edu.cn)

Received: 25 June 2024 – Discussion started: 1 August 2024
Revised: 5 November 2024 – Accepted: 13 November 2024 – Published: 28 January 2025

**Abstract.** The high-resolution ship emission inventory serves as a crucial dataset for various disciplines including atmospheric science, marine science, and environmental management. Here, we present a global high-spatiotemporal-resolution ship emission inventory at a resolution of $0.1° \times 0.1°$ for the years 2013 and 2016–2021, generated by the state-of-the-art Shipping Emission Inventory Model (SEIMv2.2). Initially, the annual 30 billion Automatic Identification System (AIS) data underwent extensive cleaning to ensure data validity and accuracy in temporal and spatial distribution. Subsequently, integrating real-time vessel positions and speeds from AIS data with static technical parameters, emission factors, and other computational parameters, SEIM simulated ship emissions on a ship-by-ship, signal-by-signal basis. Finally, the results were aggregated and analyzed. In 2021, the ship activity dataset established based on AIS data covered 109 300 vessels globally (101 400 vessels reported by the United Nations Conference on Trade and Development). Concerning the major air pollutants and greenhouse gases, global ships emitted $847.2 \times 10^6$ t of $CO_2$, $2.3 \times 10^6$ t of $SO_2$, $16.1 \times 10^6$ t of $NO_x$, 791.2 kt of CO, 737.3 kt of HC (hydrocarbon), 415.5 kt of primary $PM_{2.5}$, 61.6 kt of BC (black carbon), 210.3 kt of $CH_4$, and 45.1 kt of $N_2O$ in 2021, accounting for 3.2 % of $SO_2$, 14.2 % of $NO_x$, and 2.3 % of $CO_2$ emissions from all global anthropogenic sources, based on the Community Emissions Data System (CEDS). Due to the implementation of fuel-switching policies, global ship emissions of $SO_2$ and primary $PM_{2.5}$ saw a significant reduction of 81.3 % and 76.5 % in 2021 compared to 2019, respectively. According to the inventory results, the composition of vessel types contributing to global ship emissions remained relatively stable through the years, with container ships consistently contributing $\sim 30$ % of global ship emissions. Regarding vessel age distribution, the emission contribution of vessels built before 2000 (without Tier standards) has been declining, dropping to 10.2 % in 2021, suggesting that even a complete phase-out of these vessels would have limited potential for reducing $NO_x$ emissions in the short term. On the other hand, the emission contribution of vessels built after 2016 (meeting Tier III standard) kept increasing, reaching 13.3 % in 2021. Temporally, global ship emissions exhibited minimal daily fluctuations. Spatially, high-resolution emission characteristics of different vessel types were delineated. Patterns of ship emission contributions by different types of vessels vary among maritime regions, with container ships predominant in the North and South Pacific, bulk carriers predominant in the South Atlantic, and oil tankers prevalent in the Arabian Sea. The distribution characteristics of ship emissions and intensity also vary significantly across different maritime regions. Our dataset, which is accessible at https://doi.org/10.5281/zenodo.10869014 (Wen et al., 2024), provides a daily breakdown by vessel type and age; it is available for broad research purposes, and it will provide a solid data foundation for fine-scale scientific research and shipping emission mitigation.

Published by Copernicus Publications.

## 1 Introduction

Ships carry over 80 % of global trade volume (UNCTAD, 2024). Employing heavy fuel oil, ships emit significantly more atmospheric pollutants than diesel cars each year (Corbett et al., 1999; Endresen et al., 2003; Faber et al., 2020). Existing studies indicate that ship emissions of atmospheric pollutants and greenhouse gases have important environmental and climatic impacts on multiple spheres of the Earth (Browse et al., 2013; Chen et al., 2020; Diamond, 2023; Zhang et al., 2021). In terms of air quality, ships are regarded as a major source of $PM_{2.5}$ pollution in coastal cities (Liu et al., 2024; Luo et al., 2023). Recent studies show that although ship emissions have decreased due to stricter control measures in recent years, shipping-related mortality associated with long-term $PM_{2.5}$ exposure in Chinese coastal areas increased by 11.4 % from 2016 to 2020 as populations migrate towards coastal cities (Luo et al., 2024). Ship-emission-induced sulfur oxides aerosols significantly influence local climates (Liu et al., 2016; Yuan et al., 2022). With the increasing navigation in the Arctic, ship emissions of black carbon have become a focal point of research and policy debates regarding their impact on the polar ice surface (Stephenson et al., 2018; Zhang et al., 2019). Regarding their impact on marine organisms, anthropogenic emissions account for over 80 % of the utilizable nitrogen deposition in the ocean, with maritime emissions contributing to 15 % of global $NO_x$ emissions (Zhang et al., 2021). Given these facts, characterizing ship emissions is crucial for fundamental research in atmospheric, marine, and climatic sciences, etc.

The characterization of ship emissions through emission inventories stands as a pivotal and effective methodology within maritime emissions research (Liu et al., 2016; Liu et al., 2024; Wang et al., 2021). Over the past 30 years, with the improvement of ship activity data collection mechanisms, the establishment of ship emission inventories has gradually shifted from the "top-down" approach, based on fuel or power consumption statistics and empirical parameters, to the "bottom-up" approach, based on high-spatiotemporal-resolution shipping trajectory data (Eyring et al., 2010; Jasper et al., 2020; Liu et al., 2016). Currently, the establishment of high-spatiotemporal-resolution ship emission inventories based on Automatic Identification System (AIS) data has become the most popular tool for scientific research and policy management in the field of ship emissions (Johansson et al., 2017; Kramel et al., 2021; Wang et al., 2021). AIS consists of onboard equipment and shore-based and satellite-based receivers. During navigation, the onboard equipment transmits AIS signals every 2 s to several minutes, which are received by terrestrial or satellite-based AIS receivers and then transmitted in time to servers for storage. AIS messages record the ship's unique identifier and high-frequency dynamic information that changes continuously as the vessel progresses, including the vessel's MMSI code; IMO number; signal transmission time; ship's position (longitude and latitude); over-ground speed; and operational status, draft, and destination. Leveraging real-time ship speed derived from AIS data along with vessel technical specifications such as deadweight tonnage and design speed and emission factors, it is feasible to model instantaneous ship emissions and then aggregate them at a defined spatiotemporal granularity, thereby constructing a high-resolution emission inventory dataset. The advantage of this method is that the derived emission inventory does not rely on external spatiotemporal allocation parameters but retains accurate spatiotemporal information of ship emissions from AIS data (Liu et al., 2016). However, the challenge lies in the difficulty of processing AIS data, the complexity of simulating instantaneous ship emissions, and the significant computational resources required (Chen and Yang, 2024). Currently, the mainstream international ship emission inventory models based on AIS data include the Ship Traffic Emission Assessment Model (STEAM; Jalkanen et al., 2012; Johansson et al., 2017), the Shipping Emission Inventory Model (SEIM; Yi et al., 2024), the International Maritime Organization (IMO) emission inventory model (Jasper et al., 2020), and the Maritime Transport Environmental Assessment Model (MariTEAM; Kramel et al., 2021).

In this study, we established a $0.1^\circ \times 0.1^\circ$ global daily ship emission inventory for the years 2013 and 2016–2021 based on SEIMv2.2. This dataset covers five air pollutants ($NO_x$, $SO_2$, $PM_{2.5}$, CO, HC) and four greenhouse gases ($CO_2$, $CH_4$, $N_2O$, BC). Due to rigorous quality control, the ship emission inventory established by SEIM possesses high information density, allowing for analysis across multiple dimensions, such as fleet structure and spatiotemporal characteristics. Initially, we conducted meticulous data cleaning and rigorous quality control on the commercially obtained global ship AIS data to establish a reliable ship activity dataset. Subsequently, employing the latest emission factor and real-time engine power simulation methods for ships, SEIMv2.2 computed instantaneous ship emissions, integrating multiple quality control techniques such as interpolation processing for sparse routes and safety margin considerations to ensure the accuracy of ship emission simulation. Finally, we aggregated ship emissions from different temporal and spatial scales, as well as from different types and ages of ships. The derived high-resolution global shipping emission inventory could serve as input data for climate or atmospheric chemistry models.

The next section will elucidate the methodology and factors employed in establishing our high-resolution ship emission inventory. Section 3.1 compares our results with previous global ship emission inventories. Section 3.2 analyzes the temporal sequence of global ship emissions. Section 3.3 examines the spatial distribution characteristics of global ship emissions. Section 4 provides information regarding our

dataset and data availability. Finally, Sect. 5 presents the conclusion.

## 2 Methods

### 2.1 Ship Emission Inventory Model (SEIM)

#### 2.1.1 General principles

The Shipping Emission Inventory Model (SEIM) was first established by Liu et al. (2016) based on the idea of the disaggregated dynamic method. Driven by AIS data, combined with each vessel's registration information, SEIM realized real-time, vessel-by-vessel shipping emission simulations. SEIM is suitable for the establishment of multi-scale shipping emission inventories with applications in regions (Liu et al., 2016; Wang et al., 2021) and ports (Fu et al., 2017). SEIM has undergone two major updates: SEIMv2.0 (Wang et al., 2021) and SEIMv2.2 (this study). Compared to SEIMv2.0, SEIMv2.2 features three key improvements. (1) IMO numbers are employed as the primary identifier to match AIS data and the Ship Technical Specifications Database (STSD), and for those that cannot be matched, MMSI (Maritime Mobile Service Identity) codes are used as the secondary identifier. We found that the matching rate of the ship archive database established in previous years could significantly decrease when applied to new years. This is because when ships are leased or AIS equipment is replaced, the MMSI code often changes, while the IMO code remains constant. Therefore, using the IMO code as the first-choice identifier ensures more accurate matching of AIS data and static ship information. See Sect. 2.1.2 for details. (2) The formula for calculating the main engine load has been revised to include parameterized correction schemes for draft, meteorological conditions, and hull fouling. Additionally, a main engine load maximum limit of 98 % is set to consider the navigation safety of ships. Refer to Sect. 2.1.3 for further details. (3) The ship emission factors are comprehensively updated according to the Fourth Green House Gases Study by IMO (Jasper et al., 2020), and a black carbon calculation module has been integrated. This update also integrates the Emission Control Area (ECA) correction module directly into the calculation process, rather than applying it as a post-process adjustment. Detailed methods are provided in Sect. 2.1.4. During the development off SEIMv2.2, SEIMv2.1 was derived, which only updated the emission factors compared to SEIMv2.0. Generally, the technical scheme of SEIMv2.2 is illustrated in Fig. 1.

The calculation process and principles of SEIMv2.2 could be described as follows: firstly, the original AIS data collected are subject to cleaning, missing data filling, etc., to establish a well-cleaned dynamic AIS database. Secondly, IMO or MMSI codes are used as unique identifiers to match AIS data with the STSD, which provides essential technical parameters such as vessel type, deadweight tonnage, main engine power rating, and design speed, to establish a comprehensive shipping activity database. For the details of STSD, refer to Wang et al. (2021). This study has incorporated information on newly built vessels from 2019 to 2021, obtained from Lloyd's Register, into the established STSD. Thirdly, a series of parameters such as emission factors, auxiliary engine and boiler output power, specific fuel consumption, low load adjustment factors, and weather and fouling factors are input for ship emission simulation. Then, the model will calculate GHGs (greenhouse gases) and air pollutant emissions for every ship by every two subsequent AIS signals. The emissions from the main engine, auxiliary engine, and boiler are simulated using the corresponding formulas presented as Eqs. (1)–(3).

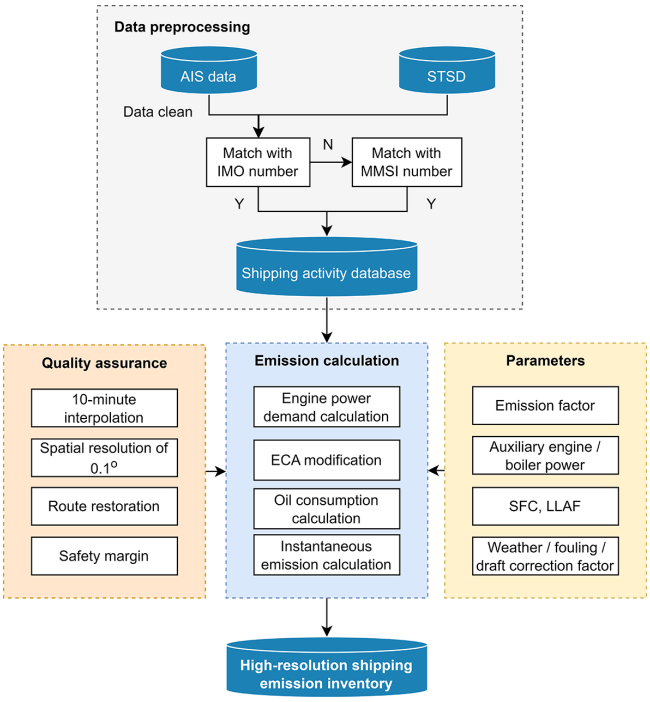


**Figure 1.** The technical scheme for SEIMv2.2.

$$E_{\mathrm{ME},i,n,p} = P_{\mathrm{ME},i,n} \times \mathrm{EF}_{\mathrm{ME},i,p} \times \mathrm{LLAF}_{i,n,p} \times \Delta T_{i,n} \times 10^{-6} \quad (1)$$

$$E_{\mathrm{AE},i,n,p} = P_{\mathrm{AE},i,n} \times \mathrm{EF}_{\mathrm{AE},i,p} \times \Delta T_{i,n} \times 10^{-6} \quad (2)$$

$$E_{\mathrm{B},i,n,p} = P_{\mathrm{B},i,n} \times \mathrm{EF}_{B,i,p} \times \Delta T_{i,n} \times 10^{-6}, \quad (3)$$

where the subscripts ME, AE, and B represent the main engine, auxiliary engine, and boiler, respectively; $i$ represents an individual ship; $n$ represents the $n$th AIS signals in the sequence, and the total number of AIS signals transmitted by the ship $i$ could be expressed using $N_i$; and $p$ represents species of GHGs or air pollutants. As for the capital letters, $E$ represents the emissions of GHGs or air pollutants (unit: t); EF is the emission factor (unit: g kW h$^{-1}$); $P$ is the output power (unit: kW); $\Delta T$ is the time interval of two subsequent AIS signals (unit: h); and LLAF is the low load adjust factor, which is applied only when the main engine load factor is lower than 20 %, consistent with our previous work. The total

emissions are calculated by summing up the emissions from all main engines, auxiliary engines, and boilers, as shown in Eq. (4).

$$E_{i,p} = \sum_{n=1}^{N_i-1} E_{i,n,p} = \sum_{n=1}^{N_i-1} (E_{\mathrm{ME},i,n,p} + E_{\mathrm{AE},i,n,p} + E_{\mathrm{B},i,n,p}) \quad (4)$$

During the real-time calculation, linear interpolation is applied to latitude and longitude displacement as well as time intervals where the AIS time interval is greater than 10 min. AIS latitude and longitude are rounded to one decimal place to ensure a spatial resolution of $0.1° \times 0.1°$. In the Chinese coastal region, route restoration technology is applied to restore routes crossing land (refer to Wang et al., 2021). If, due to anomalies in speed or other factors, the main engine load exceeds 100 %, it is capped at 98 % for safety navigation considerations. Finally, the high-resolution emission inventory generated by SEIM could be aggregated and analyzed from various angles such as emission structure, temporal variations, and spatial distribution, depending on study demands.

### 2.1.2 AIS data cleaning

AIS data provide high-density vessel activity data, including time, speed, and latitude–longitude coordinates. This study collected global shore-based and satellite-based AIS data, with an average annual signal count of approximately 30 billion. Due to irregular or erroneous information entry at ports or on vessels, as well as interference from complex marine environments, weather conditions, and terrain, AIS data may suffer from errors, duplicates, and losses. To enhance the accuracy of emission inventory calculations, this study conducted meticulous cleaning of AIS data. Firstly, to ensure data validity, we filter AIS message records that met all of the following conditions: (1) annual AIS signal count greater than 10, (2) speed over ground less than 50 kn, (3) longitudes ranging from −180 to 180° and latitudes ranging from −90 to 90°, and (4) the timestamp of AIS signals within the target year.

Secondly, for temporal anomaly cleaning, signals with excessively long time intervals are filtered out. According to the International Convention for the Safety of Life at Sea (SOLAS), vessels are required to maintain continuous transmission of AIS signals throughout the year, except for specific reasons permitted by regulations. Therefore, vessels theoretically maintain a high frequency of signal transmission during navigation. Taking the year 2021 as an example, Fig. S3 in the Supplement reveals a distinct bimodal distribution of original AIS signals, with peaks occurring around 300 s and 2 h. The peak of around 300 s corresponds to the high-frequency interval for shore-based AIS equipment to receive signals, while the peak of around 2 h mainly originates from satellite AIS signals. Statistical analysis shows that 99.6 % of signal time intervals are within 8000 s. However, the total duration of these AIS signal intervals accounts for only 16 % of all AIS signals, indicating the presence of extremely long consecutive signal intervals in the AIS data. This may be due to vessel docking for repairs or AIS equipment malfunctions. To minimize uncertainty in emission calculations caused by these signals, this study filters out signals with time intervals exceeding 7 d, which are not included in the emission calculations.

Thirdly, for spatial distribution anomaly cleaning, AIS data distributed on land are filtered out. Spatial distribution of the annual original AIS signal (Fig. S4) revealed a significant number of signals deviating from shipping routes near the 0 and 120° meridians, located over Asia, Europe, and Africa. Further analysis indicated that such abnormal signal points are caused by misaligned field information or data loss. To minimize the interference of these abnormal signals on emission calculations, this study employs the following cleaning methods:

1. For ships matched by IMO codes, signals with speeds $> 50$ kn or consecutive latitude–longitude spans $> 20°$ are removed.

2. For ships matched by MMSI codes, signals with speeds $> 40$ kn or latitude–longitude spans $> 8°$ are excluded.

3. Signals located on land areas are excluded.

Figure S4 simultaneously presents the spatial distribution of the cleaned AIS signals, revealing that signals on land near the 0 and 120° meridians have been eliminated while retaining signals on major navigable rivers in North America, South America, and Eurasia.

Fourthly, to ensure the reliability of ship technical parameter data matching, the AIS data are subsequently aggregated and identified with IMO numbers and MMSI numbers. AIS data comprise static AIS data and dynamic AIS data. Static AIS data include time, MMSI numbers, and IMO numbers but do not contain latitude and longitude information. Dynamic AIS data contain MMSI numbers and latitude and longitude information. This study integrates the static AIS data and dynamic AIS data by matching their common MMSI numbers. It is found that approximately 84 % of the MMSI numbers in dynamic information could be matched with a unique valid seven-digit IMO number. However, some ships may change their MMSI codes multiple times within a year. Data with MMSI code changes more than 10 times are excluded from emission calculations.

### 2.1.3 Engine power demand

Engine power demand is crucial for emission calculations. For the main engine, its real-time output power is related to the main engine load, which can be depicted in real time by changes in the ship's speed over ground obtained from AIS data. According to the propeller law, the main engine load

factor is the cube of the ratio of the ship's actual speed to its design speed (Liu et al., 2016). Additionally, some studies indicate that factors such as draft, hydrological and weather conditions, and hull fouling also influence the main engine load (Chen and Yang, 2024; Emmens et al., 2021; Fu et al., 2022). Regarding draft factors, the Jasper et al. (2020) corrects the main engine load using real-time draft data from AIS. However, draft fields in commercial AIS data are often manually recorded by crew members, leading to low accuracy and a large number of zero values. As for hydrological and weather conditions, wind and waves could increase engine power demand through friction and shear resistance. Johansson et al. (2017) adopt a method based on a real-time ship heading and weather field, which requires substantial computational resources and introduces greater uncertainty by the weather field. Additionally, the accumulation of micro- and macro-organisms on ship surfaces increases power demand to overcome resistance, and existing studies often use fixed parameters to correct the influence. This study introduces parameterization schemes to correct the influence of draft, weather, and hull fouling. Based on the ships' payload utilization calculation algorithm in IMO (2015), this study estimates the average drafts for different types of vessels, with specific values provided in Table S1 in the Supplement. The correction coefficients for weather influences ($\eta_w$) are based on Jasper et al. (2020), also presented in Table S1. The correction coefficient for fouling influences ($\eta_f$) is set to 0.917. Specifically, the formula for calculating the real-time power of the main engine in SEIMv2.2 can be found in Eq. (5).

$$P_{ME,i,n} = P_{ref,i} \times LF_{i,n} = \frac{P_{ref,i} \times \left(\frac{D_i}{D_{ref,i}}\right)^{0.66} \times \left(\frac{v_{i,n}}{v_{ref,i}}\right)^3}{\eta_w \times \eta_f}, \quad (5)$$

where $P_{ref,i}$ represents the maximum engine output power (unit: kW) of the main engine of the ship $i$, and $LF_{i,n}$ represents the main engine load factor of the ship $i$ at the $n$th AIS signals in the sequence. $D_i$ represents the average draft; $D_{ref,i}$ represents the designed draft; $v_{i,n}$ represents the speed over ground (unit: knot) of the ship $i$ at the $n$th AIS signals in the sequence; $v_{ref,i}$ represents the design speed (unit: knot) of ship $i$, obtained from the static technical profiles; and $\eta_{w,i}$ represents the weather correction factor and $\eta_{f,i}$ the fouling correction factor, both of which are unitless.

For auxiliary engines and boilers' power demand, this study adopts the recommended values from the IMO Fourth and Third Greenhouse Gas Study reports. Due to the lack of information, this study did not consider the impact of other auxiliary devices on board, such as solar panels, wind sails, waste heat recovery systems, and carbon capture, utilization and storage (CCUS) systems, on vessel energy consumption. These systems are not significant contributors to overall vessel energy consumption currently (DNV, 2022). However, with the ongoing trends of energy efficiency improvements, the impact of these systems on vessel energy utilization could be transformative in the future (Kersey et al., 2022).

### 2.1.4 Emission factors

The emission factors applied by SEIMv2.0 is mainly based on the IMO Third Greenhouse Gas Study (Smith et al., 2014) as well as the National Standard for General Diesel Fuel of the People's Republic of China (Wang et al., 2021). In this study, we updated the emission factors based on the IMO Fourth Greenhouse Gas Study (Jasper et al., 2020) and therefore accompanying technical modification. Firstly, emission factors of conventional air pollutants ($SO_2$, $NO_x$, $PM_{2.5}$, CO, HC) and GHGs ($CO_2$, $CH_4$, $N_2O$) were updated. $CO_2$, $SO_2$, and $PM_{2.5}$ are considered typical species whose emission factors are highly dependent on the chemical component of fuels. Table. S2 represents the emissions factors based on fuel consumption for $CO_2$, $SO_2$, and $PM_{2.5}$. Energy-based emission factors are calculated based on fuel-based emission factors as well as specific fuel consumption (SFC; unit: kW h per kg fuel), using Eq. (6):

$$EF_e = EF_f \cdot SFC, \quad (6)$$

where SFC represents the fuel consumption per unit of work performed by a ship, mainly decided by the fuel calorific value (kW h per kg fuel) and engine efficiency (%). During the operation of ships, energy efficiency could be considered a quadratic function of the load factor of the main engine, generally with the optimal load factor of 80 %. Equation (7) is applied to calculate the SFC for main engines based on the SFC under the optimal operating condition ($SFC_{base}$) and main engine load of the ship $i$.

$$SFC_{ME,i} = SFC_{base,ME,i} \cdot (0.455 \cdot LF_i^2 - 0.71 \cdot LF_i + 1.28) \quad (7)$$

Generally, newer ships have a lower $SFC_{base}$ than older ships due to the improvement of engine and auxiliary engine efficiency (Sou et al., 2022). The LNG (liquefied natural gas) fleet also has a lower $SFC_{base}$ value than conventional fuel. SFC of auxiliary engines and boilers ($SFC_{AE|B,i}$) is not subject to the main engine load, so $SFC_{AE|B,base,i}$ is directly applied with no main engine load adjustment. Values of $SFC_{base}$ are exhibited in Table S3.

Combining Table S2 and Eqs. (1) and (2), energy-based emission factors for the main engines of $CO_2$ and $SO_2$ as a function of the main engine load could be derived, as exhibited in Fig. S1 in the Supplement. It could be noted that although marine gas oil (MGO) has a higher carbon content compared to heavy fuel oil (HFO), its lower SFC results in a lower energy-based $CO_2$ emission factor. Figure S2 illustrates a comparison between two algorithms employed in SEIMv2.0, which utilizes uniform emission factors for all operational conditions, and SEIMv2.2, which incorporates load-dependent emission factors. We selected a typical oil

tanker with deadweight tonnage of 7562 t and examined its hourly carbon emissions from 1 to 15 July 2019. It is evident that, at anchorage or berth, the hourly emissions estimated by SEIMv2.2 are generally higher than or equal to those of the previous SEIMv2.0. When the vessel is cruising, however, the overall emissions calculated by SEIMv2.2 are relatively lower compared to SEIMv2.0. Emission factors of other air pollutants and GHGs in this study are shown in Tables S4 and S5.

### 2.2 Data source and quality control

#### 2.2.1 AIS data coverage

The AIS-observed data obtained in this study amounted to approximately 30 billion per year, while the processed AIS signals after cleaning and interpolation averaged about 4–5 billion per year, with an average annual operating time of approximately 5–7 $\times 10^6$ h, as shown in Table 1. In comparison to Johansson et al. (2017), the AIS signal volume in this research is slightly lower, possibly due to comprehensive quality control measures in data reduction and filtering, which removed a significant number of signals with inadequate validity, abnormal time or spatial distribution, and insufficient reliability. It can be observed that with the increasing prevalence of AIS equipment, the quantity of AIS signals is on the rise. However, the operating time does not necessarily increase in proportion to the signal quantity. The operating time decreased by 3.8 % in 2020 compared to 2019 and increased by 4.5 % in 2021 compared to 2020, probably influenced by the pandemic,

Taking 2021 as an example, the spatial distribution of AIS signals after cleaning and time interpolation is illustrated in Fig. 2. The spatial coverage of cleaned AIS signals is extensive, with signals primarily concentrated along major shipping routes such as the coastal regions of east Asia, the Malacca Strait–Cape of Good Hope route, the Mediterranean route, and the Black Sea route, effectively depicting the trajectories of major shipping lanes.

#### 2.2.2 Global fleet composition

Table 2 presents the global fleet structure obtained through matching AIS data with STSD in 2021. This study covers 14 vessel types, including major cargo vessels, passenger ships, and fishing vessels, along with a category labeled "others", comprising research vessels, rescue ships, and work vessels, among others. Since the others category primarily consists of small coastal vessels, its contribution to emissions is minor. It is important to note that the United Nations Conference on Trade and Development (UNCTAD) definition of others differs from this study's categorization. According to UNCTAD 2021 classification, other ships include liquefied petroleum gas carriers, liquefied natural gas carriers, parcel (chemical) tankers, specialized tankers, reefers, offshore supply vessels, tugboats, dredgers, cruise ships, ferries, and other non-cargo

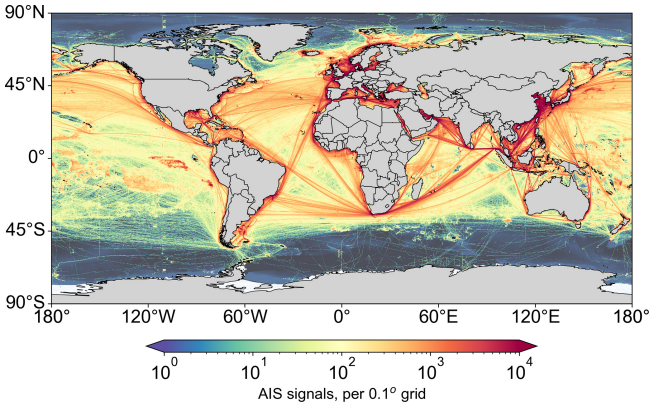


**Figure 2.** The spatial distribution of global AIS signals in 2021. Maps are made with Natural Earth.

ships. Moreover, it should be noted that the fleet obtained in this study comprises vessels with certain activity levels (annual AIS signals exceeding 10), whereas UNCTAD statistics do not consider vessel activity. This discrepancy might lead to comparatively lower results in this study.

Overall, the discrepancies between the global fleet statistics in this study and those of UNCTAD are not substantial. In terms of vessel numbers, this study reached 109 300 in 2021, slightly higher than UNCTAD's 101 400. The total deadweight tonnage amounts to 1989.9 $\times 10^6$ t, slightly lower than UNCTAD's 2136.2 $\times 10^6$ t. Among the fleet obtained in this study, vessels matched by IMO numbers reach 62 900, contributing 57.5 % of vessel count and 95.4 % of deadweight tonnage. Vessels matched by MMSI numbers constitute a larger proportion in count (42.5 %) yet make a smaller contribution in deadweight tonnage (4.6 %), predominantly consisting of fishing vessels (which contribute 87.9 % to the vessel count matched by MMSI numbers). There is a noticeable difference in the quantity of general cargo ships and oil tankers. However, in terms of total tonnage, the container ships, general cargo ships, bulk carriers, and oil tankers show no significant differences (below 10 %) with UNCTAD, ensuring the reliability of global ship emission calculations and emission structure analysis.

## 3 Results

### 3.1 Total global shipping emissions

We established a multi-year global ship emissions inventory with temporal resolution of day and spatial resolution of 0.1° using SEIM for the years 2013 and 2016–2021. Figure 3 summarizes this study and open-source dataset of major atmospheric pollutants and greenhouse substances emitted by global shipping over the past decade. The ship emission calculation method employed in this research, which is AIS-based, aligns with the methods utilized in the EDGAR (Emissions Database for Global Atmospheric Research) in-

**Table 1.** Annual AIS signals and operating time after data cleaning.

| Year | 2013 | 2016 | 2017 | 2018 | 2019 | 2020 | 2021 |
|---|---|---|---|---|---|---|---|
| AIS signals, billion | 1.6 | 4.1 | 4.6 | 5.0 | 5.0 | 5.0 | 5.5 |
| Operating time, $\times 10^6$ h | 225.8 | 578.5 | 643.6 | 700.9 | 693.8 | 667.3 | 697.6 |

**Table 2.** Comparison of the global fleet structure of this study and the UNCTAD statistics in 2021. The fleet analyzed in this study was filtered to include vessels with an annual AIS signal count greater than 10.

| | Number of vessels, thousand | | | | Total deadweight tonnage, $\times 10^6$ t | | | |
|---|---|---|---|---|---|---|---|---|
| | This study | | | UNCTAD | This study | | | UNCTAD |
| Vessel type | Match with IMO number | Match with MMSI number | Total | | Match with IMO number | Match with MMSI number | Total | |
| Auto carrier | 0.8 | 0.1 | 0.8 | | 15.3 | 0.9 | 16.2 | |
| Bulk carrier | 11.1 | 0.6 | 11.7 | 12.3 | 842.3 | 27.6 | 869.9 | 913.2 |
| Chemical tanker | 4.7 | 0.3 | 5.0 | | 100.5 | 4.5 | 105.0 | |
| Container | 4.2 | 0.3 | 4.5 | 5.4 | 218.8 | 14.4 | 233.2 | 281.8 |
| Cruise | 0.2 | 0.1 | 0.2 | | 0.1 | 0.0 | 0.1 | |
| Fishing ship | 5.1 | 40.8 | 45.8 | | 4.0 | 5.8 | 9.7 | |
| General cargo | 6.9 | 0.8 | 7.7 | 20.0 | 66.4 | 4.4 | 70.7 | 77.9 |
| LNG | 0.3 | 0.0 | 0.3 | | 19.3 | 0.2 | 19.5 | |
| LPG | 1.2 | 0.1 | 1.2 | | 19.0 | 0.8 | 19.9 | |
| Miscellaneous | 12.3 | 1.4 | 13.7 | | 76.1 | 6.5 | 82.6 | |
| Ocean tug | 7.0 | 0.9 | 7.9 | | 13.4 | 1.6 | 15.0 | |
| Oil tanker | 5.4 | 0.4 | 5.8 | 11.5 | 505.3 | 22.2 | 527.5 | 619.3 |
| Reefer | 0.5 | 0.0 | 0.5 | | 3.5 | 0.2 | 3.7 | |
| Ro-Ro | 3.0 | 0.6 | 3.6 | | 11.8 | 1.7 | 13.5 | |
| Others | 0.5 | 0.0 | 0.5 | 52.2 | 3.1 | 0.0 | 3.1 | 243.9 |
| Total | 62.9 | 46.4 | 109.3 | 101.4 | 1899.1 | 90.8 | 1989.9 | 2136.2 |

ventory and the IMO Fourth Greenhouse Gas Study released in 2020, while the CEDS inventory is established based on a top-down fuel-based approach (McDuffie et al., 2020). Methodologically, our study is more comparable to the research conducted by EDGAR and IMO, with the results from the CEDS inventory as a reference. It is important to note that SEIM has undergone two major version updates. The data of different versions are presented in Fig. S3. Figure 3 presents the integrated results for ease of comparison with other studies. Specifically, the results for 2013 are based on SEIMv1.0, while those for 2016–2020 are based on SEIMv2.1 and those for 2021 are based on SEIMv2.2. Due to slight differences between the two versions (Fig. S5), both of which include data for 2020, the total emissions for 2020 in SEIMv2.2 were adjusted to match those in SEIMv2.1. The growth rate for 2021 was kept consistent to ensure that the data for both versions align in 2020. In terms of annual emission totals, this study's results show similarities in emission trends and total emissions compared to well-known inventories such as EDGAR and IMO. For most species, this study's results show higher annual growth rates compared to IMO and EDGAR studies. For instance, this study estimates a 6.1 % annual increase rate in global ship $CO_2$ emissions from 2016 to 2018, while IMO's study indicates only a 1.4 % annual increase for its "vessel-based" results and 0.9 % for its "voyage-based" results. In 2019 and 2020, influenced by international trade conflicts and the global pandemic, this study estimates a 5.8 % and 9.5 % year-on-year decrease in global ship $CO_2$ emissions for 2019 and 2020, respectively. In contrast, the year-on-year decrease rate estimated by EDGAR inventory is 2.1 % and 8.4 % for 2019 and 2020, respectively. Differences between studies may stem from factors such as AIS data quality, coverage of static information, and factors considered in emission calculations. In 2020, the global implementation of the fuel-switching policy led to a significant reduction in the sulfur content of ship fuel. According to SEIM, in 2020 relative to 2019, $SO_2$, $PM_{2.5}$, and BC emissions decreased by 81.9 %, 77.2 %, and 40.9 %, respectively. In 2021, following the recovery in global trade demand after the pandemic, this study estimates an increase of 3.5 % in global ship $CO_2$ emissions compared with 2020, while the EDGAR inventory estimates an increase of 5.9 %. However, the latest data on ship's atmospheric pollutants from other in-

ventories only extend to 2019, which is insufficient for comparing emission results with this study.

## 3.2 Temporal evolution

### 3.2.1 Daily shipping emissions

To compare the magnitude of changes in emissions of various atmospheric pollutants and greenhouse gases emitted by ships, Fig. 4 converts the daily ship emissions of nine species into daily relative quantities, taking the emission levels on 1 January 2016 as the reference point. Figure 4 reveals that, aside from occasional sharp declines or increases on certain dates, the daily variations in ship emissions are generally stable. This suggests that the emission simulations by SEIM exhibit continuity and stability. Ships typically cruise at constant speeds on high seas without significant diurnal or other periodic variations, so global ship emissions do not exhibit pronounced daily or seasonal fluctuations. Any anomalies such as sudden drops or spikes may be attributed to signal transmission anomalies in equipment or meteorological factors. In 2019, the reduction in ship $SO_2$ emissions compared to 2018 was slightly larger than that of other pollutants, probably attributed to the implementation of the domestic emission control area policy within 12 nmi (22.2 km) of the Chinese coast, one of the world's busiest areas for shipping activities (Chen et al., 2017), which has also been demonstrated in Fig. 7c. In Fig. 4, finer temporal patterns can be observed, such as the gradual increase in emissions during the second half of 2017 and the subsequent decrease in ship emissions in 2019 as trade conflicts intensified. In 2020, the impact of the pandemic led to two phases of decline and recovery in global ship emissions. The 2020 global fuel-switching policy also led to a significant reduction in ship $SO_2$, $PM_{2.5}$, and BC emissions. Despite the implementation of NECA policy from 2016 to 2021 (IMO, 2023), the decline in ship $NO_x$ emissions is very slow, as shown in Fig. 4, which is due to the fact that the current fleet is still predominantly composed of ships built before 2016 (accounting for more than 85 %, as shown in Fig. 6). The slow pace of fleet renewal makes it more challenging to achieve substantial reductions in $NO_x$ emissions from ships currently. It is worth noting that $CH_4$ emissions exhibit relatively large daily changes and increase throughout the 6 years. The primary source of $CH_4$ emissions is LNG ships. The daily fluctuations in ship $CH_4$ emissions are mainly due to variations in LNG ship activities. Although LNG ships are currently relatively few in number, their quantity is increasing as the demand for low-carbon ships grows steadily (Gronholm et al., 2021).

### 3.2.2 Multi-dimensional structure

Figure 5 displays the daily $CO_2$ emissions classified by vessel type. From 2016 to 2021, container ships, bulk carriers, and oil tankers consistently contributed the most, accounting for 31.6 %, 18.7 %, and 14.1 % of global ship $CO_2$ emissions in 2021, respectively. The contribution of container ships increased from 30.7 % to 31.6 % from 2016 to 2021. Overall, there were no significant changes in the composition of vessel types over the 6 years. Vessel types reflect the types of commodities transported by sea, indicating the relative stability of the global maritime cargo structure.

Figure 6 illustrates the daily $NO_x$ emissions composed by the vessel construction period. The construction year of vessels determines the $NO_x$ emission standards followed by their engine (IMO, 2008). From 2016 to 2021, vessels complying with Tier I standards (built during the year 2000–2010) consistently contributed over 50 % of ship $NO_x$ emissions, while those complying with Tier II standards (built during the year 2010–2015) contributed approximately half of Tier I emissions. As the majority of ship $NO_x$ emissions come from Tier I- and Tier II-standard vessels, global ship $NO_x$ emissions are expected to remain at current levels in the short term without further control measures. However, it is noteworthy that the contribution of vessels over 20 years old (built-year $\leq 2000$) to global ship $NO_x$ emissions has gradually decreased, from 14.4 % in 2016 to 10.2 % in 2021. Meanwhile, the contribution of newly built vessels (built-year $\geq 2016$) to global ship $NO_x$ emissions steadily increased from 3.5 % in 2019 to 13.3 % in 2021.

## 3.3 Spatial characteristics

### 3.3.1 High-resolution patterns

Based on latitude and longitude coordinates in AIS signals, the ship emissions dataset was spatially aggregated into grids, resulting in the global spatial distribution of ship emissions. Figure 7 depicts the $SO_2$ emissions from global ships in $0.1° \times 0.1°$ grids. The regions with a high intensity of ship $SO_2$ emissions include east Asia, south Asia, Europe, the Persian Gulf, the Mediterranean, and the western coast of Europe. The intensive ship emissions along major global shipping routes are clearly visible, such as the routes connecting east Asia through the Malacca Strait, the Suez Canal, and the Strait of Hormuz to western European countries (the "Europe–Middle East–Far East route"); the Strait of Gibraltar; the Strait of Hormuz; the critical passage connecting the Pacific Ocean and the Atlantic Ocean; and the Panama Canal. Comparing the spatial distribution of ship $SO_2$ emissions in different years, noticeable reductions in emissions are observed in ECAs such as North America, the Gulf of Mexico, the North Sea, and the Baltic Sea comparing the ship $SO_2$ emissions distribution in 2013 and 2016. A significant reduction in emissions is also observed in the Domestic Emission Control Area (DECA) comparing the ship $SO_2$ emissions distribution in 2016 and 2019. In 2021, the implementation of the global low-sulfur fuel policy resulted in a significant overall reduction in ship $SO_2$ emissions spatially compared with 2019. The spatial distribution of ship $SO_2$ emissions in

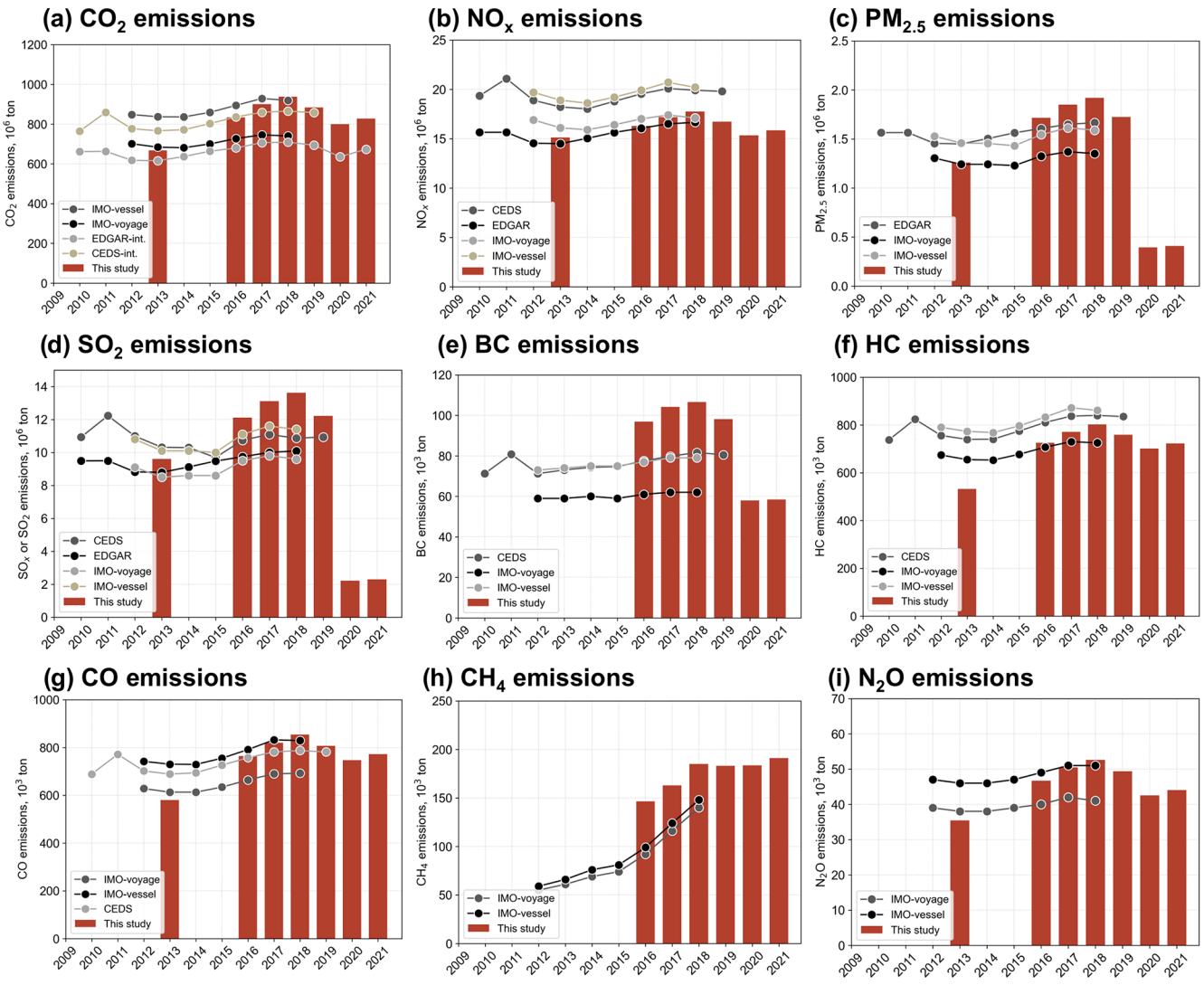


**Figure 3.** Global trends in shipping emissions from 2010 to 2021. Data sources include the IMO Fourth Greenhouse Gas Study (Jasper Faber, 2020), where IMO- Voyage results were calculated using a voyage-based method and IMO-Vessel on a vessel-based algorithm; the Community Emissions Data System (McDuffie et al., 2020); and the Emissions Database for Global Atmospheric Research (Crippa et al., 2021).

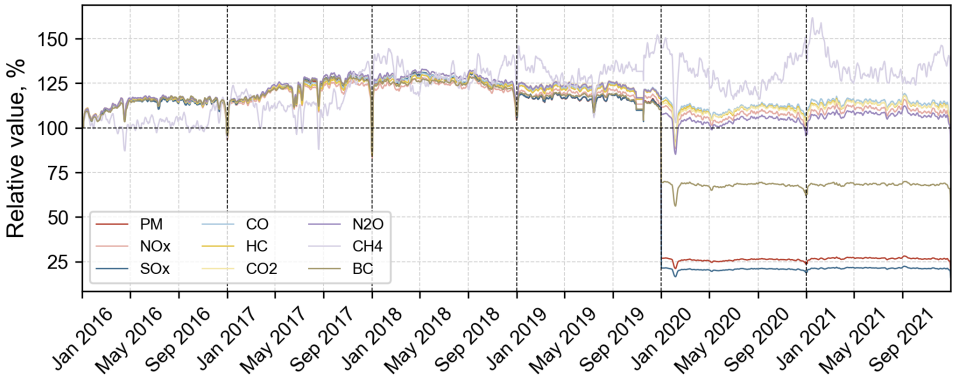


**Figure 4.** Daily global shipping air pollutants and GHG emissions from 2016 to 2021. With 1 January 2016 as the reference point, the 5 d moving average of daily relative emissions is displayed.

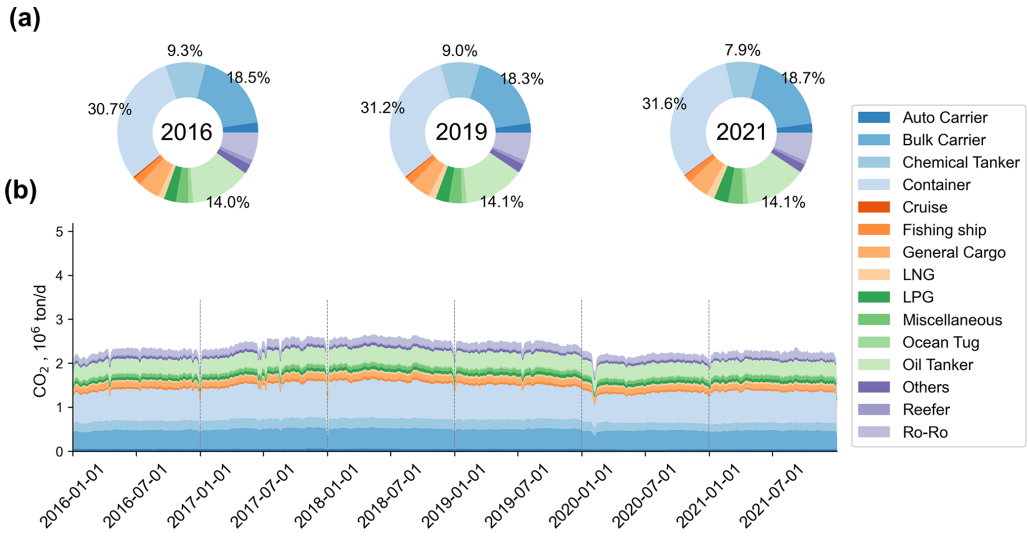


**Figure 5.** Composition of global ship $CO_2$ emissions by vessel type from 2016 to 2021. **(a)** The percentage contribution of emissions by vessel type for the years 2016, 2019, and 2021 and **(b)** the 5 d moving average of daily emissions for different vessel types.

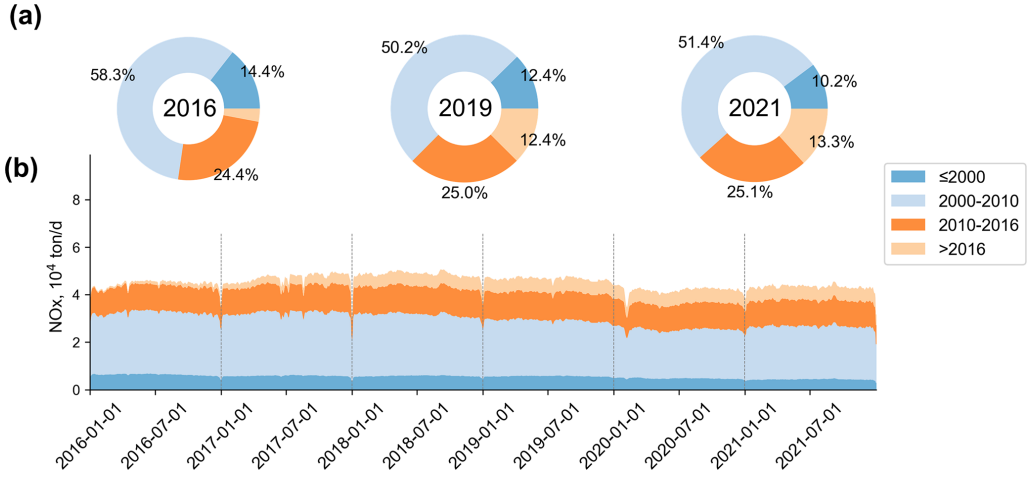


**Figure 6.** Composition of global ship $NO_x$ emissions by vessel construction year from 2016 to 2021. **(a)** The percentage contribution of emissions by vessels constructed in different periods for the years 2016, 2019, and 2021 and **(b)** the 5 d moving average of daily emissions for vessels constructed in different periods.

different years demonstrates that SEIMv2.2 effectively responds to $SO_2$ emission control policies.

### 3.3.2 Spatial disparities of vessel composition

Distinct disparities in spatial distribution are evident between freight vessels and non-freight vessels in Fig. 8. Emissions from container ships, bulk carriers, and oil tankers are concentrated in major international shipping lanes. In contrast, emissions from non-transport vessels such as fishing vessels are more widely distributed in non-lane open-sea areas. According to this study, in 2021, fishing vessels contributed 1.6 % to global ship $CO_2$ emissions, with their emissions mainly concentrated in the North Sea, Baltic Sea, Yellow Sea, and South Pacific. In recent years, studies have utilized fine satellite data to reveal significant fishing vessel activities that had not been publicly tracked worldwide (Paolo et al., 2024). The emissions from those fishing vessels remain unknown. Therefore, the emissions from fishing vessels presented in this study should be considered highly uncertain and are not discussed in the following sections.

The spatial distribution of emissions varies across different vessel types, leading to disparities in the composition of vessel types in different maritime regions. The division of global maritime regions is based on the International Hydrographic Organization (IHO) standards (https://iho.int/, last access: 14 January 2024). Figure 9 illustrates the composition of vessel types in the top 14 regions with the highest

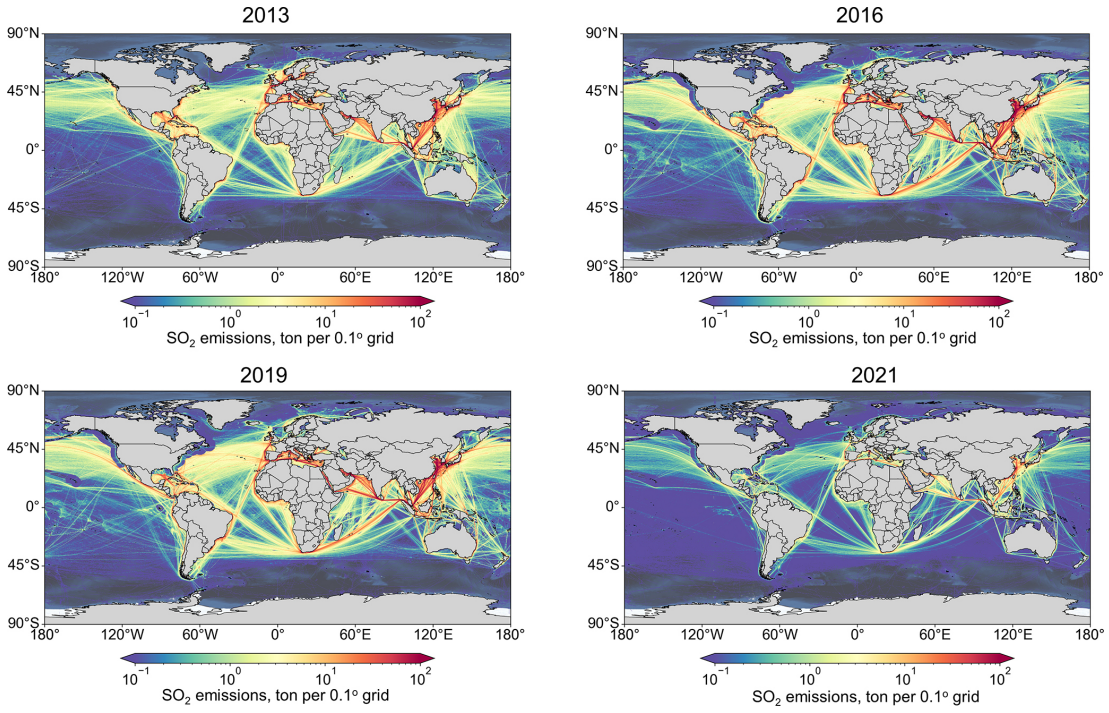


**Figure 7.** Spatial distribution of global ship $SO_2$ emissions in different years.

$CO_2$ emissions globally in 2021, with their combined emissions accounting for almost 80 % of the total global emissions. In the pie charts for each region, vessel types contributing over 10 % of emissions are labeled. It is observed that container ships contribute significant emissions in the North Pacific Ocean, South China Sea, and East China Sea, accounting for 49.4 %, 37.4 %, and 38.7 %, respectively, well above the global average (31.6 %). Regions with high contributions from bulk carriers are mainly distributed in the Southern Hemisphere, such as the Indian Ocean (40.7 %) and South Atlantic (34.9 %). Ro-Ro vessels exhibit high emissions proportions near Europe, with percentages of 38.7 % in the Baltic Sea, 19.3 % in the North Sea, and 18.1 % in the Mediterranean. Oil tankers contribute 28.5 % of emissions in the Arabian Sea, probably attributed to countries like Saudi Arabia and Iran, rich in oil and gas resources, generating substantial shipping emissions during exports to other countries.

### 3.3.3 Emission intensity

Since there are significant differences in the area of $0.1° \times 0.1°$ grids at different latitudes, ship emissions within each grid are standardized into emission intensity, i.e., emissions per unit area (unit: $t\,km^{-2}$). Taking ship $CO_2$ emissions as an example, Fig. 10 illustrates the total ship $CO_2$ emissions and emission intensity in major maritime regions in 2021. The top 30 maritime regions with the highest $CO_2$ and $NO_x$ emissions, accounting for approximately 96 % of the total global ship emissions, are listed and arranged in descending order of total emissions. It is important to note that the South/North Pacific, South and North Atlantic, and Indian Ocean cover a vast area (about 75 % of the total maritime area), most of which has little or no ship navigation. Calculating the total average emission intensity for these regions would weaken their significance, so they are not discussed here. Among other maritime regions, the South China Sea has the highest total ship $CO_2$ and $NO_x$ emissions. As a vital route for maritime trade between east Asia, Europe, and Africa, the South China Sea exhibits prominent ship traffic density globally. Additionally, the eastern Mediterranean basin, the Arabian Sea, the East China Sea, the Philippine Sea, and the North Sea also have relatively significant total emissions. Generally, maritime regions with high $CO_2$ emissions also have relatively high $NO_x$ emissions. Although the order of maritime regions with lower emissions differs slightly, overall consistency is observed. There are significant differences between maritime regions with high emissions and those with high emission intensity. The top five maritime regions with the highest ship $CO_2$ emission intensity are the Yellow Sea, the Persian Gulf, the East China Sea, the North Sea, and the Tyrrhenian Sea. The top five for $NO_x$ emission intensity are also the same maritime regions. These regions are coastal areas or busy maritime routes with intensive ship emissions, which warrants attention in environmental management in the future.

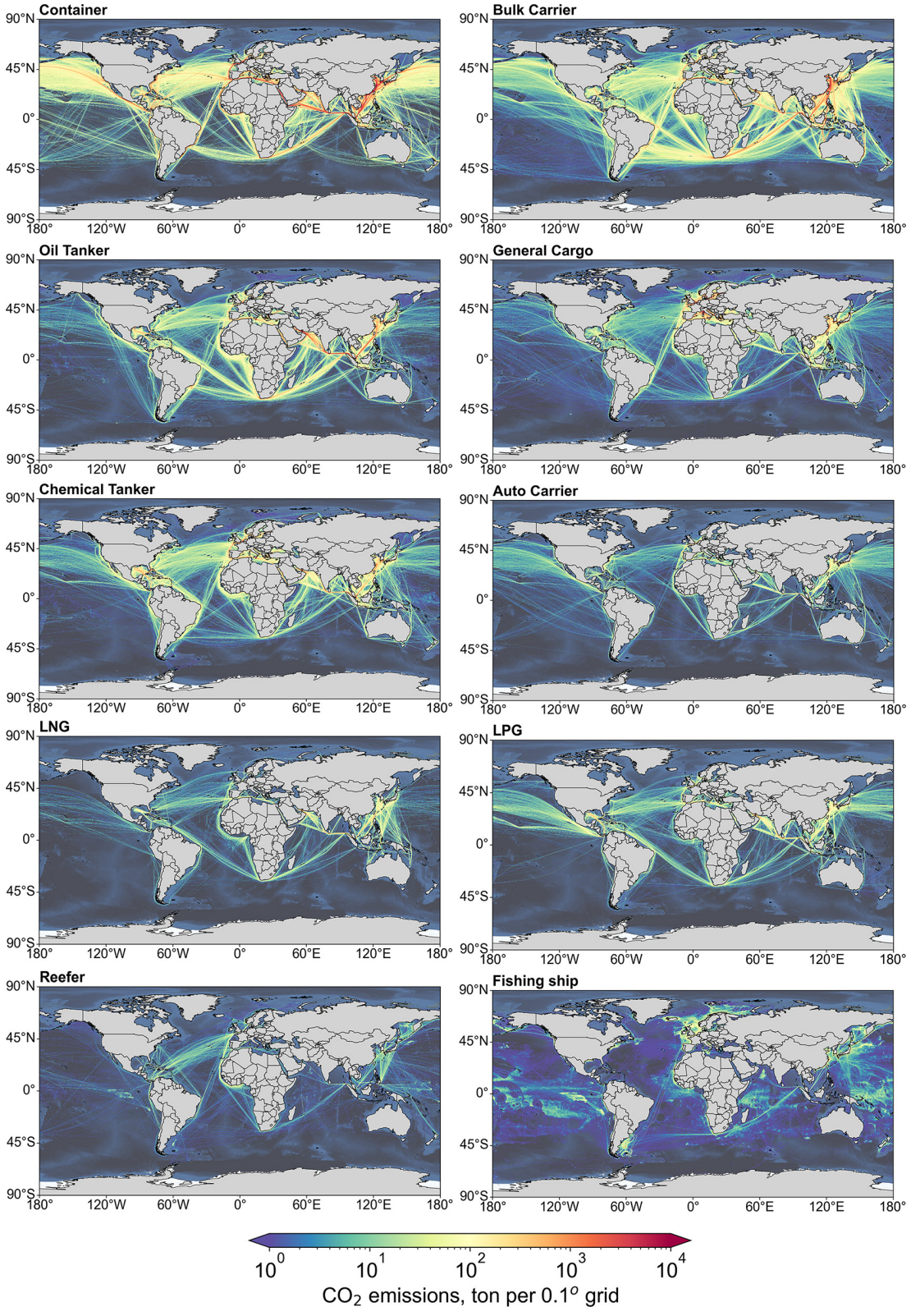


**Figure 8.** Spatial distribution of $CO_2$ emissions from different types of vessels in 2021.

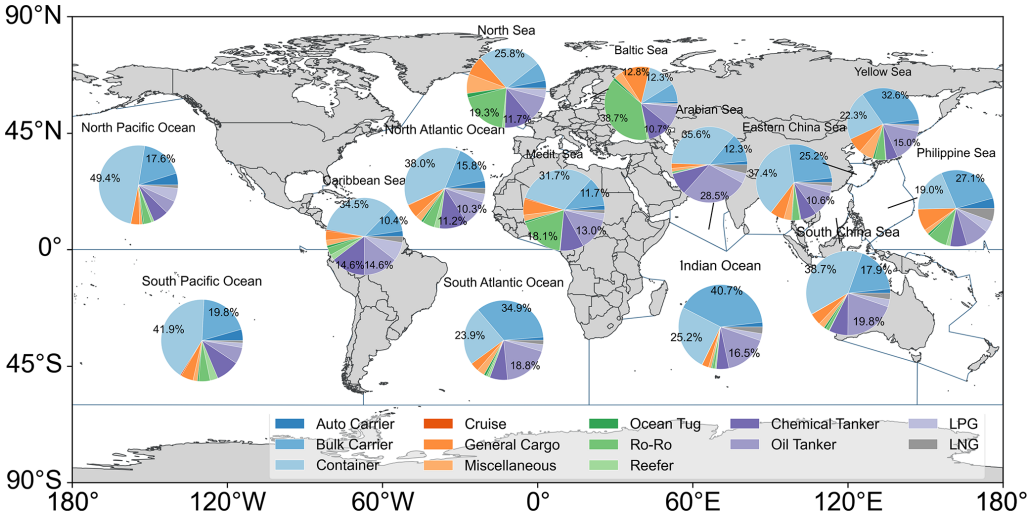


**Figure 9.** Ship $CO_2$ emissions composition in different maritime regions globally in 2021 (excluding fishing ships and others).

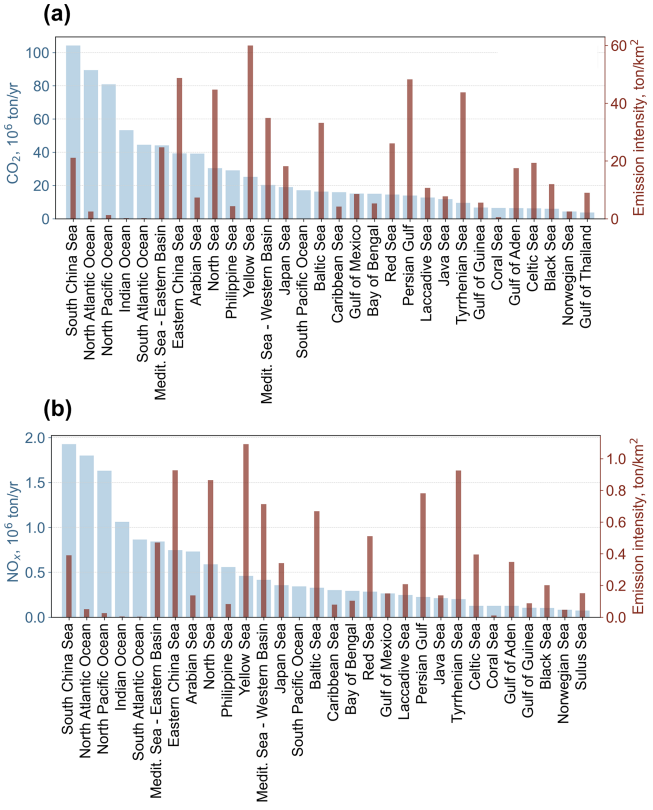


**Figure 10.** Global ship **(a)** $CO_2$ and **(b)** $NO_x$ emission and emission intensities in different maritime regions in 2021.

## 4 Data availability

Shipping emission data described in this paper can be accessed at Zenodo under https://doi.org/10.5281/zenodo.10869014 (Wen et al., 2024).

## 5 Conclusions

Utilizing SEIM, we developed a high-resolution ship emission inventory covering the period from 2013 to 2016–2021 globally, encompassing five atmospheric pollutants ($NO_x$, $SO_2$, $PM_{2.5}$, CO, HC) and four greenhouse gases ($CO_2$, $CH_4$, $N_2O$, BC). With a temporal resolution of day and spatial resolution of 0.1° × 0.1°, our inventory revealed novel insights into global ship emission characteristics.

In terms of annual emissions, our inventory exhibits consistency in temporal trends and emission magnitudes compared to mainstream inventory datasets including EDGAR, CEDS, and IMO. According to this study and the global anthropogenic emission inventory by Hoesly Rachel (2024), ship emissions contributed 12.3 % of $SO_2$, 14.0 % of $NO_x$, and 2.5 % of $CO_2$ to global anthropogenic emissions in 2019 and 3.2 % of $SO_2$, 14.2 % of $NO_x$, and 2.3 % of $CO_2$ to global anthropogenic emissions in 2021. Over the years, ship $CO_2$, $NO_x$, CO, HC, and $N_2O$ emissions showed a declining trend due to the impacts of the 2019 trade conflict (year-on-year decrease rate 5.4 %–6.2 %) and the 2020 pandemic (year-on-year decrease rate 7.4 %–13.8 %), with a subsequent rebound in 2021 as international trade increased (year-on-year increase rate 3.1 %–3.6 %). $SO_x$, PM, and BC emissions were significantly influenced by gradually implemented ECA policies and the 2020 low-sulfur fuel-switching policy. $SO_x$ and PM emissions in 2021 were 80.9 % and 76.0 % of those in 2019, and BC emissions were 38.7 % of those in 2019. $CH_4$

emissions exhibited an increasing trend over the years, growing by 43.5 % in 2021 compared to 2016.

Regarding emission composition, container ships consistently constituted the primary source of global ship $CO_2$ emissions, contributing over 30 % annually and steadily increasing, followed by bulk carriers, oil tankers, and chemical tankers. The proportion of emissions contributed by new ships increased annually from 3.5 % in 2016 to 13.3 % in 2021. However, Tier I and Tier II ships still dominate ship $NO_x$ emissions. Currently, Tier III standards only apply to vessels operating in North American Emission Control Areas. Achieving a significant reduction in global ship $NO_x$ emissions still requires extensive advancements in ship engine technology and follow-up regulatory measures worldwide.

As for spatial characteristics, ship emissions were particularly significant in east Asia, south Asia, and Europe, with busy shipping routes such as the western Europe–Middle East–Far East route, the Strait of Malacca, the Strait of Gibraltar, the Strait of Hormuz, and the Panama Canal showing the highest emission intensities. The regions with the highest $CO_2$ and $NO_x$ ship emission intensities were the Yellow Sea, the Persian Gulf, the East China Sea, the North Sea, and the Tyrrhenian Sea. These are not only areas with the highest emission intensity but also coastal regions with dense populations and ecosystems vulnerable to pollution. This suggests that these regions should be prioritized in environmental management efforts for improving air quality, protecting marine ecosystems, and mitigating climate. Furthermore, influenced by the types of commodities transported and the countries involved in trade, significant differences in ship emission characteristics exist across different regions. SEIM enables the analysis of the heterogeneity of spatial distributions of ship emissions. In terms of vessel type composition, container ships significantly exceeded the global average in ship $CO_2$ emissions contributions in the North Pacific, East China Sea, and South China Sea. Regions with high proportions of emissions from bulk carriers were mainly located in the Southern Hemisphere, such as the Indian Ocean, South Pacific, and South Atlantic. Emissions from oil tankers were high in the Arabian Sea and the Persian Gulf. The findings on the spatial heterogeneity of global ship emissions offer insights into region-specific management. In addition, since many high-emission regions include transboundary areas, such as the South China Sea and the Mediterranean, where maritime traffic connects multiple countries, effective mitigation in these regions will require international cooperation.

Despite the complex quality control processes employed in this study, uncertainties still persist in the aspects of AIS data accuracy, emission factors, and so on. In the next steps, more work should be done to reduce the uncertainties in the bottom-up ship emission evaluation model, including integrating latest methods and multi-source data to improve the accuracy of AIS data quality control and gathering more studies on recent ship emission factors to cover more ship size and operating status, as well as involving multiple data sources such as satellite data to validate the results. Overall, SEIM offers a globally multi-year, high-spatiotemporal-resolution ship emission inventory that provides reliable and detailed data, which could support foundational research across disciplines such as atmospheric science, environmental science, and geoscience. Meanwhile, this dataset could also provide scientific support for facilitating shipping emission mitigation in the future.

**Supplement.** The supplement related to this article is available online at: https://doi.org/10.5194/essd-17-277-2025-supplement.

**Author contributions.** WY and XW designed the research and wrote the manuscript, HL reviewed and revised the manuscript, and TH contributed to the modelling. ZL and ZL contributed to data analysis. KH and HL provided insights into the research design. All authors contributed to the writing.

**Competing interests.** The contact author has declared that none of the authors has any competing interests.

**Disclaimer.** Publisher's note: Copernicus Publications remains neutral with regard to jurisdictional claims made in the text, published maps, institutional affiliations, or any other geographical representation in this paper. While Copernicus Publications makes every effort to include appropriate place names, the final responsibility lies with the authors.

**Acknowledgements.** This work was supported by the National Natural Science Foundation of China (grant nos. 42325505 and 42401199), the National Key Research and Development Program of China (no. 2023YFC3705604 and no. 2022YFC3704200), and the China Postdoctoral Science Foundation (no. 2023M730142). We also acknowledge the Harvard-China Project on Energy, Economy and Environment and thank Chris P. Nielsen from Harvard University, for his suggested revisions to this paper.

**Financial support.** This research has been supported by the National Natural Science Foundation of China (grant nos. 42325505 and 42401199), the National Key Research and Development Program of China (grant nos. 2023YFC3705604 and 2022YFC3704200), and the China Postdoctoral Science Foundation (grant no. 2023M730142).

**Review statement.** This paper was edited by Xingchen (Tony) Wang and reviewed by Sijia Dong and one anonymous referee.

## References


Browse, J., Carslaw, K. S., Schmidt, A., and Corbett, J. J.: Impact of future Arctic shipping on high-latitude black carbon deposition, Geophys. Res. Lett., 40, 4459–4463, https://doi.org/10.1002/grl.50876, 2013.

Chen, D., Wang, X., Li, Y., Lang, J., Zhou, Y., Guo, X., and Zhao, Y.: High-spatiotemporal-resolution ship emission inventory of China based on AIS data in 2014, Sci. Total Environ., 609, 776–787, https://doi.org/10.1016/j.scitotenv.2017.07.051, 2017.

Chen, D., Fu, X., Guo, X., Lang, J., Zhou, Y., Li, Y., Liu, B., and Wang, W.: The impact of ship emissions on nitrogen and sulfur deposition in China, Sci. Total Environ., 708, 134636, https://doi.org/10.1016/j.scitotenv.2019.134636, 2020.

Chen, X. and Yang, J.: Analysis of the uncertainty of the AIS-based bottom-up approach for estimating ship emissions, Mar. Pollut. Bull., 199, 115968, https://doi.org/10.1016/j.marpolbul.2023.115968, 2024.

Corbett, J. J., Fischbeck, P. S., and Pandis, S. N.: Global nitrogen and sulfur inventories for oceangoing ships, J. Geophys. Res.-Atmos., 104, 3457–3470, https://doi.org/10.1029/1998jd100040, 1999.

Crippa, M., Guizzardi, D., Solazzo, E., Muntean, M., Schaaf, E., and Monforti-Ferrario, F.: GHG emissions of all world countries – 2021 Report, Luxembourg, https://doi.org/10.2760/173513, 2021.

Diamond, M. S.: Detection of large-scale cloud microphysical changes within a major shipping corridor after implementation of the International Maritime Organization 2020 fuel sulfur regulations, Atmos. Chem. Phys., 23, 8259–8269, https://doi.org/10.5194/acp-23-8259-2023, 2023.

DNV: Maritime Forcast to 2050, Germany, https://www.dnv.com/maritime/publications/maritime-forecast/ (last access: 16 January 2025), 2022.

Emmens, T., Amrit, C., Abdi, A., and Ghosh, M.: The promises and perils of Automatic Identification System data, Expert Syst. Appl., 178, 114975, https://doi.org/10.1016/j.eswa.2021.114975, 2021.

Endresen, O., Sorgard, E., Sundet, J. K., Dalsoren, S. B., Isaksen, I. S. A., Berglen, T. F., and Gravir, G.: Emission from international sea transportation and environmental impact, J. Geophys. Res.-Atmo., 108, 4560, https://doi.org/10.1029/2002jd002898, 2003.

Eyring, V., Isaksen, I. S. A., Berntsen, T., Collins, W. J., Corbett, J. J., Endresen, O., Grainger, R. G., Moldanova, J., Schlager, H., and Stevenson, D. S.: Transport impacts on atmosphere and climate: Shipping, Atmos. Environ., 44, 4735–4771, https://doi.org/10.1016/j.atmosenv.2009.04.059, 2010.

Fu, M., Liu, H., Jin, X., and He, K.: National- to port-level inventories of shipping emissions in China, Environ. Res. Lett., 12, 11, https://doi.org/10.1088/1748-9326/aa897a, 2017.

Fu, X., Chen, D., Guo, X., Lang, J., and Zhou, Y.: Improving the estimation of ship emissions using the high-spatiotemporal resolution wind fields simulated by the Weather Research and Forecast model: A case study in China, J. Ind. Ecol., 26, 1871–1881, https://doi.org/10.1111/jiec.13278, 2022.

Gronholm, T., Makela, T., Hatakka, J., Jalkanen, J. P., Kuula, J., Laurila, T., Laakso, L., and Kukkonen, J.: Evaluation of Methane Emissions Originating from LNG Ships Based on the Measurements at a Remote Marine Station, Environ. Sci. Technol., 55, 13677–13686, https://doi.org/10.1021/acs.est.1c03293, 2021.

Hoesly Rachel, S. S.: CEDS v_2024_04_01 Release Emission Data (v_2024_04_01), Zenodo [data set], https://doi.org/10.5281/zenodo.10904361, 2024.

IMO: Emission Control Areas (ECAs) designated under MARPOL Annex VI., UK, 2023.

IMO: Amendents to the techincal code on control of emission of nitrogen oxides from marine diesel engines, UK, 2008.

IMO: Further technical and operational measures for enhancing the energy efficiency of international shipping, UK, 2015.

Jalkanen, J.-P., Johansson, L., Kukkonen, J., Brink, A., Kalli, J., and Stipa, T.: Extension of an assessment model of ship traffic exhaust emissions for particulate matter and carbon monoxide, Atmos. Chem. Phys., 12, 2641–2659, https://doi.org/10.5194/acp-12-2641-2012, 2012.

Jasper, F., Shinichi, H., Shuang, Z., Paula, P., and Bryan, C.: Forth IMO Greenhouse gas study, London, UK, https://www.imo.org/en/OurWork/Environment/Pages/Fourth-IMO-Greenhouse-Gas-Study-2020.aspx (last access: 16 January 2025), 2020.

Johansson, L., Jalkanen, J.-P., and Kukkonen, J.: Global assessment of shipping emissions in 2015 on a high spatial and temporal resolution, Atmos. Environ., 167, 403–415, https://doi.org/10.1016/j.atmosenv.2017.08.042, 2017.

Kersey, J., Popovich, N. D., and Phadke, A. A.: Rapid battery cost declines accelerate the prospects of all-electric interregional container shipping, Nature Energy, 7, 664–674, https://doi.org/10.1038/s41560-022-01065-y, 2022.

Kramel, D., Muri, H., Kim, Y., Lonka, R., Nielsen, J. B., Ringvold, A. L., Bouman, E. A., Steen, S., and Strømman, A. H.: Global Shipping Emissions from a Well-to-Wake Perspective: The MariTEAM Model, Environ. Sci. Technol., 55, 15040–15050, https://doi.org/10.1021/acs.est.1c03937, 2021.

Liu, H., Fu, M., Jin, X., Shang, Y., Shindell, D., Faluvegi, G., Shindell, C., and He, K.: Health and climate impacts of ocean-going vessels in East Asia, Nat. Clim. Change, 6, 1037–1041, https://doi.org/10.1038/nclimate3083, 2016.

Liu, H., Yi, W., Jalkanen, J.-P., Luo, Z., Majamäki, E., Matthias, V., Moldanová, J., Shi, Z., and He, K.: Atmospheric impacts and regulation framework of shipping emissions: achievements, challenges and frontiers, Fundamental Research, https://doi.org/10.1016/j.fmre.2024.02.013, online first, 2024.

Luo, Z., He, T., Yi, W., Zhao, J., Zhang, Z., Wang, Y., Liu, H., and He, K.: Advancing shipping NOx pollution estimation through a satellite-based approach, PNAS Nexus, 3, pgad430, https://doi.org/10.1093/pnasnexus/pgad430, 2023.

Luo, Z., Lv, Z., Zhao, J., Sun, H., He, T., Yi, W., Zhang, Z., He, K., and Liu, H.: Shipping-related pollution decreased but mortality increased in Chinese port cities, Nature Cities, 1, 295–304, https://doi.org/10.1038/s44284-024-00050-8, 2024.

McDuffie, E. E., Smith, S. J., O'Rourke, P., Tibrewal, K., Venkataraman, C., Marais, E. A., Zheng, B., Crippa, M., Brauer, M., and Martin, R. V.: A global anthropogenic emission inventory of atmospheric pollutants from sector- and fuel-specific sources (1970–2017): an application of the Community Emissions Data System (CEDS), Earth Syst. Sci. Data, 12, 3413–3442, https://doi.org/10.5194/essd-12-3413-2020, 2020.

Paolo, F. S., Kroodsma, D., Raynor, J., Hochberg, T., Davis, P., Cleary, J., Marsaglia, L., Orofino, S., Thomas, C., and Halpin, P.: Satellite mapping reveals extensive industrial activity at sea, Nature, 625, 85–91, https://doi.org/10.1038/s41586-023-06825-8, 2024.

Smith, P., Jalkanen, P., Anderson, A., Corbett, J., Faber, J., and Hanayama, S.: Third IMO GHG Study, London, UK, 2014.

Sou, W. S., Goh, T., Lee, X. N., Ng, S. H., and Chai, K.-H.: Reducing the carbon intensity of international shipping – The impact of energy efficiency measures, Energ. Policy, 170, 113239, https://doi.org/10.1016/j.enpol.2022.113239, 2022.

Stephenson, S. R., Wang, W., Zender, C. S., Wang, H., Davis, S. J., and Rasch, P. J.: Climatic Responses to Future Trans-Arctic Shipping, Geophys. Res. Lett., 45, 9898–9908, https://doi.org/10.1029/2018GL078969, 2018.

THE United Nations Conference on Trade and Development (UNCTAD): Review of Maritime Transport, United States, https://unctad.org/publication/review-maritime-transport-2023 (last access: 16 January 2025), 2024.

Wang, X., Yi, W., Lv, Z., Deng, F., Zheng, S., Xu, H., Zhao, J., Liu, H., and He, K.: Ship emissions around China under gradually promoted control policies from 2016 to 2019, Atmos. Chem. Phys., 21, 13835–13853, https://doi.org/10.5194/acp-21-13835-2021, 2021.

Wen, Y., Xiaotong, W., Tingkun, H., Huan, L., Luo, Z., and Kebin, H.: Global shipping emissions for the years 2013 and 2016–2021, Zenodo [data set], https://doi.org/10.5281/zenodo.10869014, 2024.

Yi, W., He, T., Wang, X., Soo, Y. H., Luo, Z., Xie, Y., Peng, X., Zhang, W., Wang, Y., Lv, Z., He, K., and Liu, H.: Ship emission variations during the COVID-19 from global and continental perspectives, Sci. Total Environ., 954, 176633, https://doi.org/10.1016/j.scitotenv.2024.176633, 2024.

Yuan, T., Song, H., Wood, R., Wang, C., Oreopoulos, L., Platnick, S. E., von Hippel, S., Meyer, K., Light, S., and Wilcox, E.: Global reduction in ship-tracks from sulfur regulations for shipping fuel, Sci. Adv., 8, eabn7988, https://doi.org/10.1126/sciadv.abn7988, 2022.

Zhang, C., Shi, Z., Zhao, J., Zhang, Y., Yu, Y., Mu, Y., Yao, X., Feng, L., Zhang, F., Chen, Y., Liu, X., Shi, J., and Gao, H.: Impact of air emissions from shipping on marine phytoplankton growth, Sci. Total Environ., 769, 145488, https://doi.org/10.1016/j.scitotenv.2021.145488, 2021.

Zhang, Q., Wan, Z., Hemmings, B., and Abbasov, F.: Reducing black carbon emissions from Arctic shipping: Solutions and policy implications, J. Clean. Product., 241, 118261, https://doi.org/10.1016/j.jclepro.2019.118261, 2019.